Anatomic and functional asymmetries interactively shape human early visual cortex responses

Laura Herde

Institute of Medical Psychology and Behavioral Neurobiology, University of Tübingen, Tübingen, Germany ✉

Julia Uhl

Institute of Medical Psychology and Behavioral Neurobiology, University of Tübingen, Tübingen, Germany ✉

Karsten Rauss

Institute of Medical Psychology and Behavioral Neurobiology, University of Tübingen, Tübingen, Germany ✉

Early visual processing is surprisingly flexible even in the adult brain. This flexibility involves both long-term structural plasticity and online adaptations conveyed by top-down feedback. Although this view is supported by rich evidence from both human behavioral studies and invasive electrophysiology in nonhuman models, it has proven difficult to close the gap between species. In particular, it remains debated whether noninvasive measures of neural activity can capture top-down modulations of the earliest stages of processing in the human visual cortex. We previously reported modulations of retinotopic C1, the earliest component of the human visual evoked potential. However, these effects were selectively observed in the upper visual field (UVF). Here we test whether this asymmetry is linked to an interaction between differences in spatial resolution across the visual field and the specific stimuli used in previous studies. We measured visual evoked potentials in response to task-irrelevant, high-contrast textures of different densities in a comparatively large sample of healthy volunteers ($N = 31$) using high-density electroencephalogram. Our results show differential response profiles for upper and lower hemifields, with UVF responses saturating at higher stimulus densities. In contrast, lower visual field responses did not increase, and even showed a tendency toward a decrease at the highest density tested. We propose that these findings reflect feature- and task-specific pooling of signals from retinotopic regions with different sensitivity profiles. Such complex interactions between anatomic and functional asymmetries need to be considered to resolve whether human early visual cortex activity is modulated by top-down factors.

Introduction

Whether or not early visual cortex responses in humans are modulated by higher cognitive processes, such as learning or attention, remains under debate. On the one hand, a growing number of studies support the hypothesis that even the earliest stages of processing in the adult human visual cortex remain malleable. For example, we have shown that perceptual learning (Pourtois et al., 2008), as well as attentional load (Rauss et al., 2009; Rauss et al., 2012), can affect the C1, the earliest component of the visual evoked potential in humans (Jeffreys & Axford, 1972). In contrast, several studies conducted over the same period did not find effects of higher cognitive processes on low-level vision (Alilović et al., 2019; Baumgartner et al., 2018; Ding et al., 2014; Fu et al., 2010). In a recent review, Slotnick (2018) systematically compared studies that investigated C1 modulations by spatial attention and derived important guidelines regarding the experimental and methodologic parameters employed to assess this question. One of these guidelines is that stimuli in the upper visual field (UVF) seem to be more likely to evoke differential C1 responses as a function of spatial attention. Indeed, we repeatedly observed C1 effects only for stimulus presentation in the UVF (Pourtois et al., 2008; Rauss et al., 2009), whereas other studies did show effects of attention in the lower visual field (LVF) as well (Bao et al., 2010; Kelly et al., 2008).

Here we set out to test whether these inconsistencies, both between and within studies, could be due to a combination of stimulus differences and processing

asymmetries across the visual field. It has long been known that there are anatomic and functional differences between the upper and lower parts of the visual field (Hansen et al., 2016; Skrandies, 1987; Zhou et al., 2017; Zito et al., 2016). Asymmetries have been observed across various tasks and stimulus features. For example, psychophysiological studies showed advantages for the LVF compared with the UVF in terms of temporal and contrast sensitivities, visual acuity, spatial resolution, and hue and motion discrimination (Karim & Kojima, 2010; Levine & Mcanany, 2005; Skrandies, 1987). In fact, some authors refer to a "lower visual field advantage," highlighting the dominance of the LVF across several domains (Hagler, 2014; Lehmann & Skrandies, 1979; McAnany & Levine, 2007).

Electrophysiologically, such differences are expressed in shorter latencies and larger amplitudes for visual evoked responses following LVF stimulation (Hagler, 2014). The reasons for this advantage are not fully understood, but seem to be linked to greater receptor densities in the upper hemiretina, where input from the LVF is initially processed (Skrandies, 1987), as well as the segregation of magno- and parvocellular processing pathways (Azzopardi et al., 1996; Foxe et al., 2008; McAnany & Levine, 2007) and their subsequent routing into the dorsal and ventral visual stream, respectively (Previc, 1990; Zito et al., 2016).

The degree of asymmetric processing is likely to vary for different stimulus features and different experimental tasks. In this context, it is interesting that previous studies reporting symmetric modulations of the C1 across the horizontal meridian mostly used Gabor gratings (Bao et al., 2010; Kelly et al., 2008). In contrast, our findings of asymmetric C1 effects (Pourtois et al., 2008; Rauss et al., 2009) were obtained with large arrays of high-contrast line-elements, as classically used in studies of texture discrimination (Gais et al., 2000; Karni & Sagi, 1991; Pourtois et al., 2008). The goal of the present study was to systematically map early visual cortex responses to such texture stimuli when displayed at different densities, to assess whether asymmetric response profiles may underlie asymmetric effects of learning and attention on the C1. We note that this approach cannot establish direct comparisons between previous studies using Gabors versus textures, which differ on a number of important parameters (e.g., luminance transients, size). Nevertheless, it constitutes an important first step toward integrating disparate findings obtained with different stimuli in different task settings. Given the more extensive representation of the LVF in the human primary visual cortex (V1; Di Russo et al., 2002; Dougherty et al., 2003; Henriksson et al., 2012), we hypothesized that LVF responses would increase monotonically with stimulus density, whereas UVF responses would saturate or decline at higher densities.

To test this hypothesis, we measured C1 responses as an indicator for early visual cortex activity. The C1 is characterized by an onset latency of approximately 50 ms and usually peaks before 100 ms after stimulus onset. Moreover, it inverts polarity depending on whether the UVF or LVF is selectively stimulated. These characteristics have been interpreted as evidence for a main neural source in the primary visual cortex (V1; Jeffreys & Axford, 1972), and more recent studies using electroencephalogram (EEG) source localization methods have largely supported this idea (Capilla et al., 2016; Di Russo et al., 2002). Recent debates have focused on whether V1 activity is indeed the main source of the C1 (Ales et al., 2010; Ales et al., 2013; Kelly, Schroeder et al., 2013; Kelly, Vanegas et al., 2013). For our purposes, it is sufficient that C1 reflects the earliest reliable noninvasive handle on human early visual cortex activity.

We conducted an EEG experiment using arrays of high-contrast line elements of three different densities to selectively stimulate the upper or the lower part of the visual field while healthy human participants performed an unrelated task at fixation. In the absence of pertinent reports in the literature, we chose to sample three stimulus densities, which, if "converted" to Gabor stimuli, would largely cover the range of spatial frequencies assessed in previous studies (Bao et al., 2010; Clark et al., 1995; Poghosyan & Ioannides, 2008; Rauss et al., 2009; Rauss et al., 2012). Our results show differential response patterns between UVF and LVF across these stimulus densities: although UVF responses saturated at higher densities, LVF responses did not increase monotonically, but were actually diminished at the highest density tested. These findings indicate that known differences in anatomy and physiology between the UVF and LVF affect the earliest cortical component of the visual evoked potential.

Methods

Participants

A total number of 40 participants were tested. All subjects were right-handed and had normal or corrected-to-normal vision. None reported any history of psychiatric or neurologic disorders. Participants were recruited via advertisements at the University and throughout the city of Tübingen. Written informed consent was obtained prior to screening for exclusion criteria. The study protocol adhered to the Declaration of Helsinki and was approved by the ethics committee of the Medical Faculty at the University of Tübingen. Nine subjects had to be excluded due to bad EEG data quality (e.g., strong drifts, extensive muscle artifacts, or excessive eye movements). The remaining 31 subjects
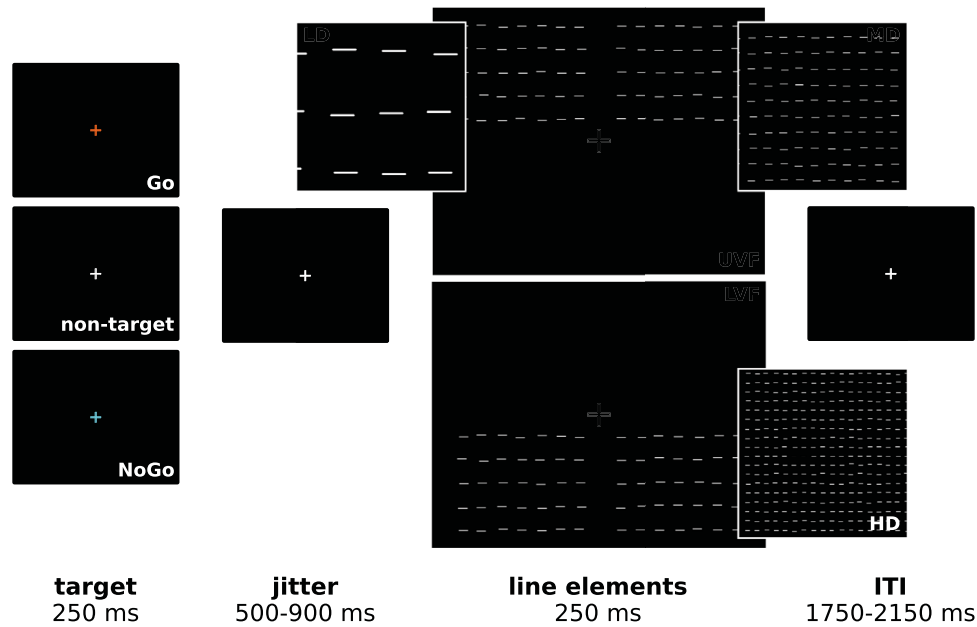
Figure 1. Structure of an experimental trial. Subjects' task was to respond with a button-press to Go-targets, and to withhold responses for NoGo targets. Following a jittered stimulus-onset asynchrony, task-irrelevant stimuli of different densities (LD, MD, HD) were presented in either the UVF or the LVF. Insets show 250 × 250 pixel cut-outs from the original stimuli. Trials were separated by variable intertrial intervals. Inset labels were not presented during the experiment.

(25 women) were aged between 18 and 36 years (median 23.5).

Stimuli

All stimuli were white ($\approx$ 96.1 cd/m^2) and shown against black background ($\approx$ 0.21 cd/m^2) on a 19-in. LED screen at 1280 × 1024 resolution and 60 Hz refresh rate using Presentation, Version 16.1 (Neurobehavioral Systems, Inc., Berkeley, CA). Viewing distance was stabilized at 57 cm using a chin-rest.

Based on protocols used in previous studies (Rauss et al., 2009; Rossi & Pourtois, 2012), we created stimulus bitmaps using the Cogent toolbox (developed by the Cogent 2000 team at the Functional Imaging Laboratory and the Institute of Cognitive Neuroscience and Cogent Graphics developed by John Romaya at the Laboratory of Neurobiology at the Wellcome Department of Imaging Neuroscience) for MATLAB (The MathWorks Inc., Natick, MA). Different stimulus densities were obtained by scaling the number of rows and columns, which constituted the line-arrays (Figure 1). To do so, each display quadrant was first tiled with square grids of three different sizes. Horizontal bars were then centered on the grid-points, with bar widths of either 1° of visual angle (low-density, LD), 0.33° (medium-density, MD), or 0.2° (high-density, HD), and a width-to-height ratio of 10:1

in all conditions. Finally, bar positions were jittered by adding offsets in both dimensions, independently drawn from a uniform distribution between 0% and 33% of bar width. This yielded stimulus arrays covering 13.1° × 10.6° of visual angle per quadrant. Both meridians (15% of display space) and the edges of the screen (7.5% of display space) remained empty. Because the bars were centered on grid-points, stimuli of lower density extended slightly further into these free spaces horizontally (average difference between LD and HD = 0.4°). The area covered by line elements was comparable between conditions (3.500–3.564 square degrees per quadrant).

For each stimulus density, 34 different stimuli were created. These were presented in pseudo-randomized order, either in the UVF or the LVF (i.e., always covering two quadrants), with no more than three consecutive stimuli per location, and no more than three consecutive stimuli of the same density, to reduce adaption effects (Ofen et al., 2007).

As shown in Figure 1, each trial started with a potential target stimulus (i.e., a change of the fixation cross color) shown for 250 ms. This was followed by a fixation period jittered between 500 and 900 ms (with the mean across trials constrained to lie between 700 and 800 ms). Then peripheral lines of a pseudo-randomly selected stimulus density were shown for 250 ms in addition to the fixation cross, either in the UVF or the LVF. The next trial started after

1750–2150 ms. Jitter durations were randomly selected from a uniform distribution both for the initial fixation period and the intertrial interval.

Design and procedure

The experiment was based on a 3 (stimulus densities) × 2 (visual field locations) within-subjects design. Whenever measurements from several EEG electrodes were simultaneously analyzed, variability due to electrode locations was captured via additional repeated-measures factors.

Before the experiment, subjects were asked about their mood and physical condition. They were then prepared for EEG recording and seated in a quiet room under constant lighting conditions. The experiment consisted of nine blocks, each containing 75 trials and lasting approximately 4 minutes. To engage subjects' attention, the fixation cross changed in color for 250 ms at the beginning of a randomly selected 20% of trials. Colors were either orange or green with equal probability, and subjects were instructed to respond to one of the colors with a button press (keypad zero on a standard computer keyboard), and to withhold responding for the other color. Color-response mapping was counterbalanced across subjects. Peripheral lines were always task-irrelevant, and subjects were instructed to ignore them.

Between blocks, there was a programmed break of 30 seconds to avoid fatigue. After these breaks, participants initiated the following block via a button press and were thus free to take longer breaks if needed. The entire recording session lasted approximately 40 minutes including breaks. After finishing the experiment, subjects were debriefed and systematically questioned concerning their attention to the task and whether they experienced any distraction because of the peripherally presented stimuli.

Data recording and analyses

The EEG was recorded from 129 electrodes placed according to an adapted 10–10 system using HydroCel Geodesic Sensor Nets (Electrical Geodesics, Inc., www.egi.com). Signals were continuously sampled at 500 Hz, referenced to the vertex. Impedances were kept below 100 kilo-Ohm (kOhm), as recommended by the manufacturer. Data quality was checked throughout the experiment and electrodes with poor data quality were adjusted between blocks.

Raw data were converted and high-pass filtered (0.1 Hz) using the FieldTrip toolbox (Oostenveld et al., 2011). Using BrainVision Analyzer 2.1 (BrainProducts GmbH, Gilching, Germany), data were then low-pass filtered at 70 Hz and a notch filter was applied at 50

Hz. Breaks between experimental blocks and periods containing strong artifacts (e.g., strong drifts or muscle activity) were manually excluded before applying independent component analysis to correct ocular artifacts (blinks and saccades) and clearly identifiable other artifacts (e.g., heartbeat). After removal of artifact components, the data were back-projected into the original signal space, and any remaining artifacts were rejected semiautomatically based on the following criteria: maximal allowed voltage step, 50 µV/ms; maximal voltage differences, 200 µV/200ms; minimal/maximal allowed amplitude: $-100/+100$ µV; minimal voltage difference, 0.5 µV/100 ms. On average, $2.4\% \pm 0.55\%$ of trials per subject were excluded during these preprocessing steps. Subsequently, all channels were re-referenced to averaged mastoids, and noisy electrodes were interpolated using a fourth-order spherical-splines procedure, as implemented in BrainVision Analyzer. To calculate event-related potentials (ERPs), epochs from -200 to $+800$ ms around the onset of peripheral stimuli were extracted and baseline-corrected using the average signal between -200 and 0 ms. Averages were computed for each of the six conditions separately. Only nontarget trials were included (i.e., trials in which the fixation cross did not change color).

The C1 component was identified in each subject based on its distinct polarity, topographic properties, and latency (60–120 ms post-stimulus onset). Peak amplitudes and latencies were semiautomatically measured at single electrodes showing maximal C1 amplitude in each participant and condition, as identified by visual inspection of individual ERPs. This approach allowed us to include subjects with atypical C1 topographies. We additionally calculated analyses based on a pool of four electrodes showing maximal C1 activity across subjects, as identified by inspection of the grand average across subjects with canonical C1 topographies ($n = 21$). Results for these analyses are reported whenever they deviate from those obtained using individual maximum electrodes. Latency values for LVF responses were corrected by subtracting 8 ms, to account for the mean delay between stimulus presentation in the upper and lower half of the screen at a refresh rate of 60 Hz.

Statistical analyses were run in SPSS 21 (IBM Corp., Armonk, NY), JASP 0.10.2 (JASP Team, 2019), and R 3.5.0/Rstudio 1.1.463 (R Core Team). For analyses including values from both LVF and UVF locations, negative C1 amplitudes for the UVF were inverted. Greenhouse-Geisser correction of degrees of freedom was applied where appropriate. In these cases, we report original degrees of freedom and the correction factor ε. Maps of voltage topographies were created using the Cartool software programmed by Denis Brunet (cartoolcommunity.unige.ch).
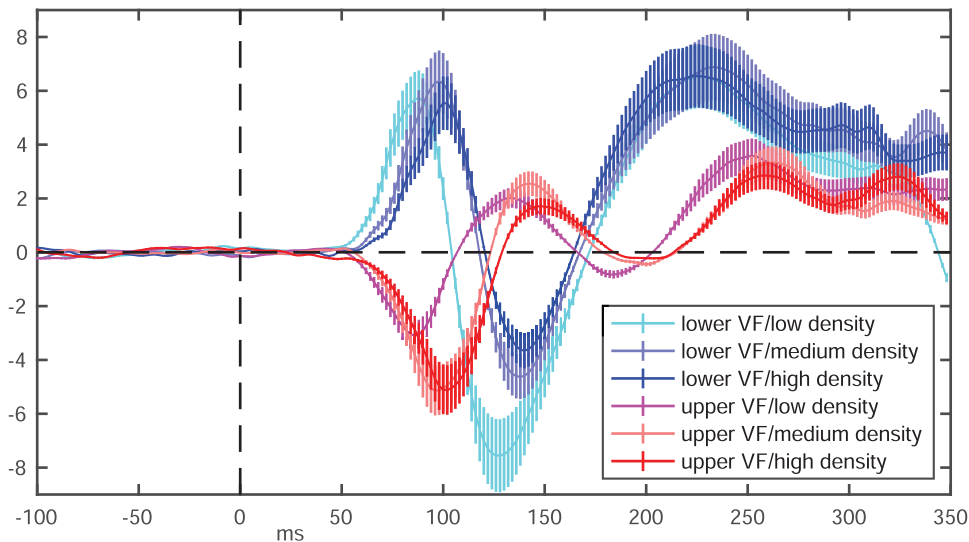
Figure 2. Event-related potential waveshapes for all six conditions. Averages were calculated based on maximum C1 electrodes per participant ($N = 31$) and condition. Note that individual differences in peak latency may lead to differences between grand-average component amplitudes as shown here and mean peak amplitudes across participants as shown in Figure 3. Epochs used for analysis extended from −200 through 800 ms around stimulus offset; a reduced interval is shown here for better display of the earliest VEP components. Error bars show *SEM* across participants. VF, visual field.

Results

Behavioral performance

Two out of 31 subjects had to be excluded from analysis of behavioral performance data due to technical problems. All of the remaining 29 subjects reached high levels of accuracy in the color detection task (percentage of correctly detected trials, mean $\pm$ *SE*, 99.3 $\pm$ 0.3%). In addition, all subjects showed low false alarm rates for distractors (1.8% $\pm$ 0.4%). Averaged reaction time for correct responses was 518 $\pm$ 12 ms, with a median of 497 ms.

Questionnaires

In questionnaires assessing current mood and physical condition, most subjects reported feeling well. One subject reported considerable sleepiness and exhaustion; another suffered from a strong headache. In both cases, behavioral performance was indistinguishable from the remaining participants and EEG data quality was high. Both subjects were thus included for analysis.

EEG data

Averages were checked for each subject individually in terms of data quality, focusing on a clearly distinguishable C1, based on the typical polarity reversal for UVF versus LVF, consistent timing, and expected topography. For all 31 subjects, a clear C1 was detected for all stimulus densities in both the LVF and UVF. Twenty-one subjects showed a canonical, central parieto-occipital C1 topography. Grand-averaged data indicated a C1 maximum at electrode POz in all six conditions, independent of whether all subjects or only those with a canonical C1 topography were included. In the LVF, C1 peaked at 80 ms for stimuli of LD, with an amplitude of 5.56 μV; at 90 ms for stimuli of MD (5.52 μV); and at 94 ms for stimuli of HD (4.61 μV). In the UVF, C1 reached its maximum at 86 ms for LD (−2.91 μV); at 96 ms for MD (−4.58 μV); and at 100 ms for HD stimuli (−4.48 μV). Figure 2 shows ERP waveshapes based on maximum C1 electrodes selected per participant and condition, as these form the basis of our primary analyses (see Data recording and analyses).

The latency values described earlier suggest substantial delays for higher stimulus densities, in accordance with known differences between magno- and parvocellular pathways conveying low and high spatial frequency information, respectively (Foxe & Simpson, 2002; Vuilleumier et al., 2003). Indeed, a 2 × 3 repeated-measures analysis of variance (ANOVA) on latency values with Location and Stimulus Density as within-subject factors showed that higher stimulus densities were associated with later C1 peaks [main effect of Stimulus Density: LD, 83 $\pm$ 1 ms; MD, 94 $\pm$ 1 ms; HD, 97 $\pm$ 1 ms; $F(2, 60) = 156.47$, $p < 0.001$]. In addition, longer delays were seen in the UVF compared with the LVF [main effect Location:

LVF, 88 ± 1 ms; UVF, 95 ± 1 ms; $F(1, 30) = 36.49$, $p < 0.001$]. Finally, we observed a significant interaction between Location and Stimulus Density, $F(2, 60) = 3.23$, $p = 0.046$. Follow-up t-tests indicated that this was due to an only marginally significant difference between UVF and LVF for LD stimuli ($p = 0.087$), whereas this difference was highly significant for MD and HD stimuli (both $p < 0.001$). The same analysis calculated only for subjects with a canonical C1 topography ($n = 21$), based on a pool of four electrodes, yielded equivalent main effects [Location: $F(1, 20) = 22.00$, $p < 0.001$; Stimulus Density: $F(2, 40) = 147.7511$, $p < 0.001$]. However, the Location × Stimulus Density interaction was only marginally significant in this case, $F(2, 40) = 3.22$, $p = 0.05$.

Turning to amplitude values, a 2×3 repeated-measures ANOVA with Location and Stimulus Density as within-subject factors indicated stronger C1 responses following stimuli presented to the LVF [main effect Location: LVF, 6.59 ± 0.40 µV; UVF, 4.95 ± 0.44 µV; $F(1, 30) = 14.15$, $p < 0.001$; note that UVF amplitude values were inverted, see Data recording and analyses]. Results also showed that C1 was maximal in response to MD stimuli [main effect Stimulus Density: LD, 5.32 ± 0.35 µV; MD, 6.15 ± 0.41 µV; HD, 5.84 ± 0.44 µV; $F(2, 60) = 4.02$, $p = 0.023$]. Importantly, UVF and LVF response profiles differed from each other, as indicated by a significant Location × Stimulus Density interaction, $F(2, 60) = 11.02$, $p < 0.001$. Follow-up t-tests between visual field locations for each stimulus density revealed significantly higher C1 amplitudes in the LVF for LD ($p < 0.001$) and MD stimuli ($p = 0.010$). No such difference was observed for HD stimuli ($p = 0.441$; *cf*. Figure 3).

A follow-up ANOVA restricted to the UVF indicated significant differences in C1 amplitudes between stimulus densities [main effect Stimulus Density: LD, -3.84 ± 0.36 µV; MD, -5.40 ± 0.55 µV; HD, -5.59 ± 0.57 µV; $F(2, 60) = 10.85$, $p < 0.001$]. Post hoc t-tests indicated lower amplitudes for LD stimuli compared with both MD and HD (LD vs. MD, $p = 0.001$; LD vs. HD, $p < 0.001$), in the absence of differences between MD and HD stimuli ($p = 0.64$). In contrast, in the LVF, there was only a marginally significant effect of Stimulus Density on C1 responses [LD, 6.79 ± 0.44 µV; MD, 6.89 ± 0.41 µV; HD, 6.08 ± 0.50 µV; $F(2, 60) = 2.70$, $\varepsilon = 0.68$, $p = 0.098$]. Post hoc t-tests indicated that this was due to higher C1 amplitudes for MD compared with HD stimuli ($p = 0.003$), in the absence of differences between LD and MD ($p = 0.80$), or between LD and HD stimuli ($p = 0.15$).

To quantify the similarity between UVF and LVF C1 responses following HD stimuli, we conducted a Bayesian ANOVA with Location and Stimulus Density
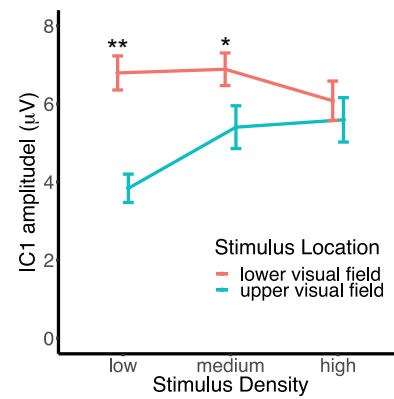

Figure 3. Average absolute C1 amplitudes $\pm$ SEM across stimulus densities and visual field locations. Peak amplitudes were measured at maximum C1 electrodes per participant ($N = 31$) and condition. Note that mean amplitudes shown here are calculated as the average of peak values measured at individually determined, maximal C1 electrodes. As this does not consider differences in latency, the values shown here are different from the grand-average peak amplitudes in Figure 2. Significance indicators are for post hoc comparisons between visual field locations for each stimulus density (*$p < 0.05$; **$p < 0.001$; Location × Stimulus Density, $p < 0.001$).

as within-subject factors, using standard priors as implemented in JASP 0.10.2. Unsurprisingly, the results were largely analogous to the classical ANOVA reported earlier, with the full model including both main effects and their interaction almost 10 times more likely than the next-best model including only Location. Analysis of individual effects indicated definite evidence for inclusion of the Location factor (Bayes Factor $[BF]_{incl} > 500,000$), moderate evidence for inclusion of Stimulus Density ($BF_{incl} = 6.87$), and strong evidence for inclusion of the Location × Stimulus Density interaction ($BF_{incl} = 24.46$). Follow-up Bayesian paired t-tests also confirmed the results of the classic t-tests reported earlier, with definite evidence for differences between UVF and LVF for both LD and MD stimuli (both $BF_{10} > 100,000$ for standard, wide, and ultrawide Cauchy priors). Importantly, the Bayesian approach allows us to quantify the probability of there being no difference between UVF and LVF C1 responses following HD stimuli. Results showed moderate evidence in favor of H_0, with $BF_{01} = 3.94$. This result remained stable across different prior widths (Figure 4).

Taken together, the results described earlier indicate important visual field anisotropies during initial processing of high-contrast textures. A potential caveat relates to the overlap between C1 and later, extrastriate components, particularly P1 (Clark et al., 1995; Slotnick, 2018). The most problematic condition is usually for LVF stimuli, as the positive-going C1 may be contaminated by the early phase of the P1. In our data,
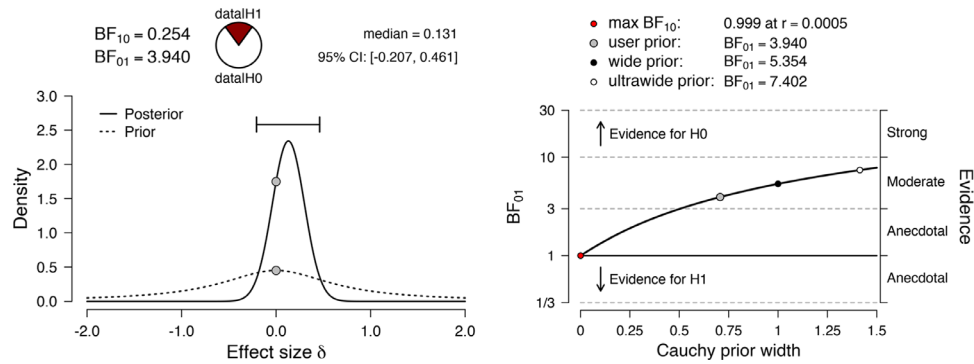
Figure 4. Bayesian paired *t*-test indicating moderate evidence in favor of equivalent lower- and upper-visual field C1 responses for HD stimuli. Left panel: The Bayes Factor (BF) in favor of the null hypothesis ($BF_{01} = 3.94$, see also graphical comparison with BF_{10} at top left) and the 95% credible interval (CI) of the median of the posterior distribution indicate that UVF and LVF amplitudes are similar. Right panel: This conclusion is confirmed by a BF robustness check across different prior settings. CI, credible interval.

we actually observe a negative component following the positive C1 after LVF stimulation. As shown in Figure 5, and in line with previous studies using similar stimuli (Clark et al., 1995; Pourtois et al., 2008; Rauss et al., 2009), this component is characterized by a circumscribed, central, parieto-occipital negativity, reminiscent of what Clark et al. (1995) termed the N90op. As detailed in the Discussion, such a polarity inversion for putatively extrastriate visual evoked potential (VEP) components is likely related to both the extent and eccentricity of the stimuli employed.

To address whether overlaps between C1 and the subsequent P1 or N90op components might have confounded the results reported earlier, we performed a repeated-measures ANOVA with factors Location and Stimulus Density, based on mean amplitudes, calculated over 20 ms time-windows around the grand-average peak latency, separately for each component and each stimulus density (UVF/P1: LD, 130–150 ms; MD, 134–154 ms; HD, 140–160 ms; LVF/N90op: LD, 118–138 ms, MD, 126–146 ms; HD, 128–148 ms). We again used absolute amplitudes (i.e., N90op values were inverted) to allow for easier interpretation of the Location factor. Results indicated differential response profiles in upper and lower visual hemifields [Location × Stimulus Density, $F(2, 60) = 24.96$, $p < 0.001$], in the context of globally higher responses in the LVF [main effect Location, $F(1, 30) = 10.61$, $p = 0.003$] and overall differences between stimuli [main effect Stimulus Density, $F(2, 60) = 10.62$, $\varepsilon = 0.802$, $p < 0.001$]. Importantly, the nature of this interaction was different from that observed for C1: follow-up *t*-tests indicated higher amplitudes in the LVF compared with the UVF for all stimulus densities (LD, $p < 0.001$; MD, $p = 0.034$; HD, $p = 0.035$, one-sided); and separate follow-up ANOVAs showed that the different stimuli elicited differential responses only in the LVF, $F(2, 60) = 38.80$, $\varepsilon = 0.815$, $p < 0.001$; UVF, $F(2, 60) = 2.23$,

$\varepsilon = 0.848$, $p = 0.126$. Post hoc tests further indicated reduced LVF responses with increasing stimulus density (all pairwise $p \leq 0.008$). Taken together, the P1 following UVF stimulation appears statistically flat, whereas the preceding C1 increases and then plateaus with increasing stimulus density. Conversely, the LVF N90op displays a steady decline across increasing stimulus densities, whereas its preceding C1 shows only moderate evidence for a decline at the highest density tested. Given these results, it appears unlikely that differences in the ascending phase of P1 and N90op would explain the differences observed for the preceding C1.

Discussion

Our results show substantial differences in early visual cortex responses to high-contrast bar arrays of different densities between the upper and lower visual hemifields. In accordance with previous behavioral (Gottwald et al., 2015; Intriligator & Cavanagh, 2001), anatomic (Dougherty et al., 2003; Henriksson et al., 2012), and functional (Liu et al., 2006; Portin et al., 1999) evidence, we observed higher C1 amplitudes in response to LVF stimulation globally. However, this global difference was gradually reduced as stimulus density increased and was not significant for stimuli of the highest density tested. Bayesian analysis supported the notion that UVF and LVF C1 responses are essentially equivalent for HD stimuli. The gradual reduction of differences between upper and lower hemifield responses was mainly driven by increased UVF responses for medium and high stimulus densities. In addition, we observed a trend for decreased LVF C1 amplitudes in response to HD stimuli.
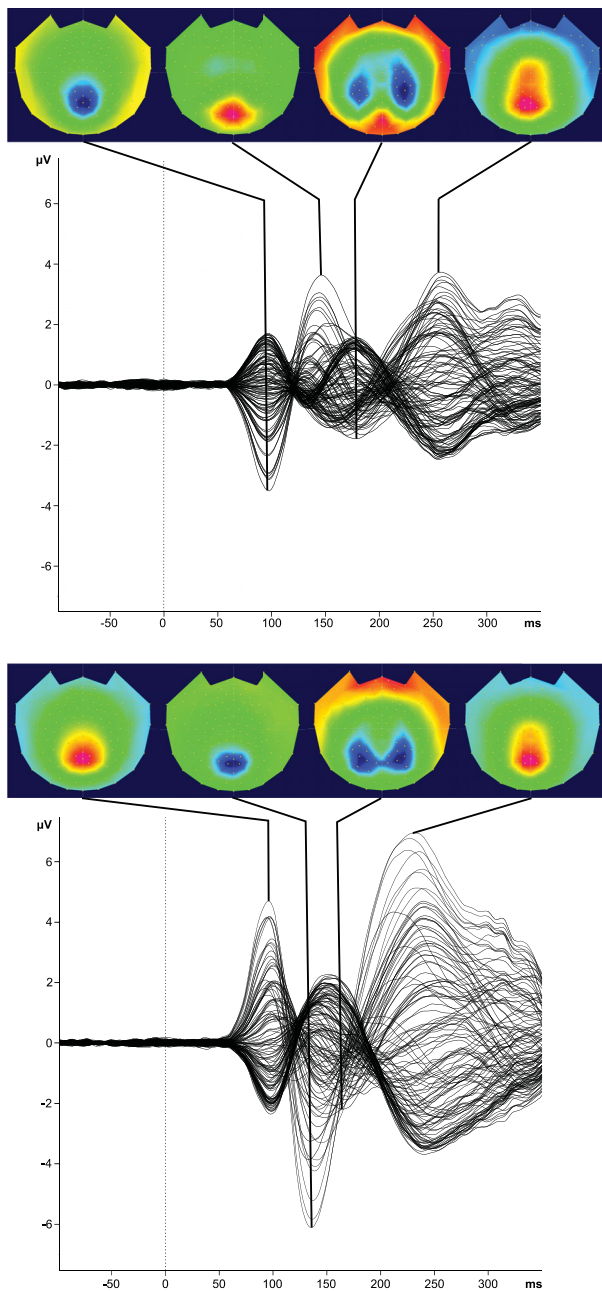
Herde, Uhl, & Rauss

Figure 5. Grand-average butterfly plots and voltage topographies for UVF (top panel) and LVF (bottom panel) stimuli of all densities and participants (*N* = 31). The expected positive C1 in the LVF (leftmost map in bottom panel) is followed by a central, occipito-parietal negativity previously described as N90op (Clark et al., 1995). This in turn is followed by a bilateral negativity of lower amplitude, with temporal and topographic characteristics similar to a canonical visual N1 (compare third maps in top and bottom panels). The subsequent component also appears largely similar to the P2 observed for UVF stimuli. All maps symmetrically scaled to the respective component's maximum amplitude.

These results partly confirm our original hypotheses, in that they show a plateau for UVF responses at higher stimulus densities. However, these data do not confirm our prediction of a monotonic increase of LVF responses for increasing stimulus densities. This unexpected finding is most likely linked to differences between our texture-like stimuli and the Gabor gratings traditionally used to assess spatial-resolution profiles. Because bar orientation was consistently horizontal in our stimuli, the predominant subjective impression is of parallel, horizontal lines. Nevertheless, the spaces between iso-oriented bars, as well as the latters' vertical jitter, would be expected to yield neural responses different from those elicited by Gabor gratings with continuous orientation axes.

Based on reports of higher cell numbers and smaller receptive fields in the upper bank of the calcarine sulcus (Silva et al., 2018), we expected a better match between higher-density stimuli and the filtering characteristics of the LVF. Specifically, more units should be activated here, and extraclassical receptive field mechanisms, such as end-stopping and flank-inhibition (Allman et al., 1985; DeAngelis et al., 1994; Ponce et al., 2017; Samonds et al., 2017; Yazdanbakhsh & Livingstone, 2006), should reduce neural responses at relatively higher stimulus densities than in the UVF. These basic anatomic considerations provide a straightforward explanation for both globally higher C1 amplitudes in the LVF, and the asymptotic behavior of the C1 seen in the UVF. However, they do not explain why we do not observe increased C1 amplitudes (and even a trend toward reduced amplitudes) in the LVF for the highest stimulus density tested.

Although the limited range of stimulus densities assessed does not allow for a complete characterization of differential response profiles, this inconsistency is nevertheless striking. There are essentially two explanations for this inconsistency: either the well-documented LVF advantage does not exist for textures; or it is masked by differential processing of UVF and LVF inputs at or before the level of the C1. The first explanation contradicts decades of research into LVF advantages in the human visual system (Karim & Kojima, 2010; Previc, 1990; Skrandies, 1987), and seems particularly unlikely because HD textures are precisely the kind of input that the LVF should be optimized for to support two-legged motion. The second explanation suggests that LVF responses to higher-density textures are dampened well below the available limits of spatial resolution. This would result in a reduction of the effective resolution in the LVF, and a corresponding lack of increases in C1 amplitudes.

From a functional point of view, such a reduction in effective resolution may be desirable for several reasons. For example, it has been argued that improved sensitivities in the LVF in primates are linked to higher acuity needed for forelimb operations in

peripersonal space (Previc, 1990, but see Hafed & Chen, 2016). For humans in particular, two-legged locomotion likely requires especially rapid and detailed peripheral monitoring of the LVF (Buckley et al., 2011; Marigold & Patla, 2008; Timmis et al., 2009). More detailed neural representations highlighting specific environmental features in circumscribed visual field locations may thus have evolved to solve particular problems (Quek & Finkbeiner, 2014; Zhang et al., 2015). However, such more detailed representations may not be necessary in all environmental settings and can sometimes even be detrimental (Carrasco & Yeshurun, 1998). Specifically, in our setup, relative suppression of inputs from the LVF may occur because stimulus discontinuities become ecologically less relevant as the size of their constituent elements decreases. Alternatively, higher-resolution tracking of the LVF may be unnecessary when both the subject and environmental stimuli are stationary. More generally, retinotopically specific specializations should not interfere with the construction of a unified percept of stimuli extending beyond their borders. This issue could arise, for example, when contours must be integrated across the horizontal meridian (Kuai & Yu, 2006; Liang et al., 2017), or when physically similar stimuli compete for attention at visual field locations with differing sensitivity profiles (Vater et al., 2017). In such cases, the construction of continuous representations may require constraining or relaxing the criteria for integrating stimulus elements in a locally specific manner.

In terms of neurophysiology, the EEG signal is thought to primarily reflect excitatory postsynaptic potentials at apical dendrites of cortical pyramidal cells (Brandeis et al., 2009), and the C1 has traditionally been regarded as an index of primary visual cortex activity (Jeffreys & Axford, 1972; Rauss et al., 2011; but see Ales et al., 2010). Inasmuch as our protocol minimized stimulus-specific top-down effects, the present data suggest that the neural mechanism underlying the apparent dampening of LVF responses at higher stimulus densities operates at the input stage to V1, or even earlier at the level of the lateral geniculate nucleus (Halassa & Kastner, 2017). Based on the functional considerations discussed earlier, we propose that more detailed neural representations of the LVF in humans are overlaid by pooling mechanisms that aggregate neural responses in a feature- and location-specific manner. Such feature-by-location-specific pooling could be achieved, for example, by differential scaling of the extent and/or gain of iso-feature suppression (Zhaoping, 2009). However, this interpretation remains speculative given that we tested only a restricted range of stimulus densities to obtain sufficient signal-to-noise ratio in a within-subjects design. Additional experiments are thus needed to verify these claims using a wider range of stimulus densities and different stimulus orientations. In a second step,

dedicated manipulations of top-down factors could be employed to test whether feature-specific pooling can be flexibly engaged, for example via top-down gating of lateral interactions in V1 inputs (Chen et al., 2014; Piëch et al., 2013; Schäfer et al., 2007).

Importantly, the C1 effects we report appear to be independent of differences emerging at later processing stages. As reviewed by Slotnick (2018), temporal overlap between C1 and the subsequent P1 component may contaminate C1 measurements. This problem is particularly pronounced for LVF stimulation, in which both components are expected to be positive. In the present study, we observe a negative VEP component following LVF C1. The response profiles of both this negative second component, as well as the P1 observed following UVF stimulation, differed substantially from those seen for the preceding C1 in the corresponding hemifield. This reduces the likelihood of C1 peak amplitudes being confounded by differences in the ascending phase of the subsequent VEP components. We and others have previously reported such an apparent polarity reversal immediately following the C1 (Clark et al., 1995; Pourtois et al., 2008; Rauss et al., 2009). The negativity following LVF C1 most likely reflects what Clark et al. (1995) originally termed the N90op: a centrally distributed, occipito-parietal negativity that was present across a wide range of positive and negative stimulus elevations in their study. Interestingly, the same component was not observed in a follow-up study (Di Russo et al., 2002), which used similar procedures, but presented stimuli at 4° eccentricity (as opposed to 8° in the original study). Integrating these results with our data based on much larger stimuli suggests that an N90op is only observed for stimuli located at or covering eccentricities substantially beyond the fovea. The fact that we observe a central N90op distribution is readily explained by our use of bilateral stimulation, whereas Clark et al. (1995) report a slight contralateral shift with unilateral stimulation. Incidentally, this may also explain why we do not observe occipito-temporal activity during the P1 interval for either UVF or LVF stimuli. More detailed mapping experiments using systematic manipulations of stimulus eccentricity and stimulus elevation would be required to determine whether N90op is consistently elicited by UVF stimuli and may often go unnoticed due to its overlap with the preceding, negative C1.

Conclusions

Our main motivation for mapping early visual cortex responses to texture-like stimuli was that we repeatedly observed asymmetric C1 modulations with similar stimuli (Pourtois et al., 2008; Rauss et al., 2009), whereas others did not report such asymmetries with

Gabor gratings (Bao et al., 2010; Kelly et al., 2008; Poghosyan & Ioannides, 2008). The results of the present experiment indicate that the nature and extent of visual field anisotropies are stimulus-specific, and thus cannot be extrapolated from, for example, localized Gabors to large-scale textures. Extending the guidelines proposed by Slotnick (2018), we would therefore argue that basic asymmetries of the visual system need to be considered when designing stimuli and tasks used to assess C1. Our findings corroborate the earlier intuition that asymmetric top-down effects on early visual cortex activity are linked to basic anatomic differences between the upper and lower hemifields. They further suggest that differential anatomic representations do not per se explain asymmetric C1 modulations. Rather, early visual cortex seems to flexibly combine representations of different granularity into a coherent whole. This flexibility may explain why it has proven difficult to pinpoint top-down modulations of early visual cortex activity in humans.

Keywords: C1, event-related potentials, visual evoked potentials, visual field anisotropies

Acknowledgments

References

Ales, J. M., Yates, J. L., & Norcia, A. M. (2010). V1 is not uniquely identified by polarity reversals of responses to upper and lower visual field stimuli. *NeuroImage, 52*(4), 1401–1409, https://doi.org/10.1016/j.neuroimage.2010.05.016.

Ales, J. M., Yates, J. L., & Norcia, A. M. (2013). On determining the intracranial sources of visual evoked potentials from scalp topography: A reply to Kelly et al. (this issue). *NeuroImage, 64*(1), 703–711, https://doi.org/10.1016/j.neuroimage.2012.09.009.

Alilović, J., Timmermans, B., Reteig, L. C., van Gaal, S., & Slagter, H. A. (2019). No evidence that predictions and attention modulate the first feedforward sweep of cortical information processing. *Cerebral Cortex, 29*(5), 2261–2278, https://doi.org/10.1093/cercor/bhz038.

Allman, J., Miezin, F., & McGuinness, E. (1985). Stimulus specific responses from beyond the classical receptive field: Neurophysiological mechanisms for local-global comparisons in visual neurons. *Annual Review of Neuroscience, 8*(1), 407–430, https://doi.org/10.1146/annurev.ne.08.030185.002203.

Azzopardi, P., Jones, K. E., & Cowey, A. (1996). Mapping of M and P projections from the lateral geniculate nucleus to the striate cortex in the macaque monkey. *Investigative Ophthalmology and Visual Science, 37*(3), 2179–2189.

Bao, M., Yang, L., Rios, C., He, B., & Engel, S. A. (2010). Perceptual learning increases the strength of the earliest signals in visual cortex. *Journal of Neuroscience, 30*(45), 15080–15084, https://doi.org/10.1523/JNEUROSCI.5703-09.2010.

Baumgartner, H. M., Graulty, C. J., Hillyard, S. A., & Pitts, M. A. (2018). Does spatial attention modulate the C1 component? The jury continues to deliberate. *Cognitive Neuroscience, 9*(1–2), 34–37, https://doi.org/10.1080/17588928.2017.1386169.

Brandeis, D., Michel, C., & Amzica, F. (2009). From neuronal activity to scalp potential fields. In C. M. Michel, T. Koenig, D. Brandeis, L. R. R. Gianotti, & J. Wackermann (Eds.), *Electrical neuroimaging*, 1–24; Cambridge: Cambridge University Press, https://doi.org/10.1017/CBO9780511596889.

Buckley, J. G., Timmis, M. A., Scally, A. J., & Elliott, D. B. (2011). When is visual information used to control locomotion when descending a kerb? *PLoS One, 6*(4), e19079, https://doi.org/10.1371/journal.pone.0019079.

Capilla, A., Melcón, M., Kessel, D., Calderón, R., Pazo-Álvarez, P., & Carretié, L. (2016). Retinotopic mapping of visual event-related potentials. *Biological Psychology, 118*, 114–125, https://doi.org/10.1016/j.biopsycho.2016.05.009.

Carrasco, M., & Yeshurun, Y. (1998). Attention improves or impairs visual performance by enhancing spatial resolution. *Nature, 396*(6706), 72–75.

Chen, M., Yan, Y., Gong, X., Gilbert, C. D., Liang, H., & Li, W. (2014). Incremental integration of global contours through interplay between visual cortical areas. *Neuron, 82*(3), 682–694, https://doi.org/10.1016/j.neuron.2014.03.023.

Clark, V. P., Fan, S., & Hillyard, S. A. (1995). Identification of early visual evoked potential generators by retinotopic and topographic analyses. *Human Brain Mapping, 2*, 170–187, https://doi.org/10.1002/hbm.460020306.

DeAngelis, G. C., Freeman, R. D., & Ohzawa, I. (1994). Length and width tuning of neurons in the cat's primary visual cortex. *Journal of Neurophysiology, 71*(1), 347–374, https://doi.org/10.1152/jn.1994.71.1.347.

Di Russo, F., Martinez, A., Sereno, M. I., Pitzalis, S., & Hillyard, S. A. (2002). Cortical sources of the early components of the visual evoked potential. *Human Brain Mapp, 15*(2), 95–111.

Ding, Y., Martinez, A., Qu, Z., & Hillyard, S. A. (2014). Earliest stages of visual cortical processing are not modified by attentional load. *Human Brain Mapping, 35*(7), 3008–3024, https://doi.org/10.1002/hbm.22381.

Dougherty, R. F., Koch, V. M., Brewer, A. A., Fischer, B., Modersitzki, J., & Wandell, B. A. (2003). Visual field representations and locations of visual areas V1/2/3 in human visual cortex. *Journal of Vision, 3*(10), 586–598, https://doi.org/10.1167/3.10.1.

Foxe, J. J., & Simpson, G. V. (2002). Flow of activation from V1 to frontal cortex in humans: A framework for defining "early" visual processing. *Experimental Brain Research, 142*(1), 139–150, https://doi.org/10.1007/s00221-001-0906-7.

Foxe, J. J., Strugstad, E. C., Sehatpour, P., Molholm, S., Pasieka, W., Schroeder, C. E., . . . McCourt, M. E. (2008). Parvocellular and magnocellular contributions to the initial generators of the visual evoked potential: High-density electrical mapping of the "C1" component. *Brain Topography, 21*(1), 11–21, https://doi.org/10.1007/s10548-008-0063-4.

Fu, S., Fedota, J. R., Greenwood, P. M., & Parasuraman, R. (2010). Dissociation of visual C1 and P1 components as a function of attentional load: An event-related potential study. *Biological Psychology, 85*(1), 171–178, https://doi.org/10.1016/j.biopsycho.2010.06.008.

Gais, S., Plihal, W., Wagner, U., & Born, J. (2000). Early sleep triggers memory for early visual discrimination skills. *Nature Neuroscience, 3*(12), 1335–1339, https://doi.org/10.1038/81881.

Gottwald, V. M., Lawrence, G. P., Hayes, A. E., & Khan, M. A. (2015). Representational momentum reveals visual anticipation differences in the upper and lower visual fields. *Experimental Brain Research, 233*(8), 2249–2256, https://doi.org/10.1007/s00221-015-4294-9.

Hafed, Z. M., & Chen, C. Y. (2016). Sharper, stronger, faster upper visual field representation in primate superior colliculus. *Current Biology, 26*(13), 1647–1658, https://doi.org/10.1016/j.cub.2016.04.059.

Hagler, D. J. (2014). Visual field asymmetries in visual evoked responses. *Journal of Vision, 14*(13):13, 1–19, https://doi.org/10.1167/14.14.13.

Halassa, M. M., & Kastner, S. (2017). Thalamic functions in distributed cognitive control. *Nature Neuroscience, 20*(12), 1669–1679, https://doi.org/10.1038/s41593-017-0020-1.

Hansen, B. C., Haun, A. M., Johnson, A. P., & Ellemberg, D. (2016). On the differentiation of foveal and peripheral early visual evoked potentials. *Brain Topography, 29*(4), 506–514, https://doi.org/10.1007/s10548-016-0475-5.

Henriksson, L., Karvonen, J., Salminen-Vaparanta, N., Railo, H., & Vanni, S. (2012). Retinotopic maps, spatial tuning, and locations of human visual areas in surface coordinates characterized with multifocal and blocked fMRI designs. *PLoS One, 7*(5), 1–18, https://doi.org/10.1371/journal.pone.0036859.

Intriligator, J., & Cavanagh, P. (2001). The spatial resolution of visual attention. *Cognitive Psychology, 43*(3), 171–216, https://doi.org/10.1006/cogp.2001.0755.

JASP Team. (2019). JASP (Version 0.10.2) [Computer software]. Retrieved from https://jasp-stats.org/.

Jeffreys, D. A., & Axford, J. G. (1972). Source locations of pattern-specific components of human visual evoked potentials. I. Component of striate cortical origin. *Experimental Brain Research, 16*(1), 1–21.

RezaulKarim, K. M., & Kojima, H. (2010). The what and why of perceptual asymmetries in the visual domain. *Advances in Cognitive Psychology/University of Finance and Management in Warsaw, 6*, 103–115, https://doi.org/10.2478/v10053-008-0080-6.

Karni, A., & Sagi, D. (1991). Where practice makes perfect in texture discrimination: Evidence for primary visual cortex plasticity. *Proceedings of the National Academy of Sciences of the United States of America, 88*(11), 4966–4970.

Kelly, S. P., Gomez-Ramirez, M., & Foxe, J. J. (2008). Spatial attention modulates initial afferent activity in human primary visual cortex. *Cerebral Cortex, 18*(11), 2629–2636, https://doi.org/10.1093/cercor/bhn022.

Kelly, S. P., Schroeder, C. E., & Lalor, E. C. (2013). What does polarity inversion of extrastriate activity tell us about striate contributions to the early VEP? A comment on Ales et al. (2010). *NeuroImage, 76*, 442–445, https://doi.org/10.1016/j.neuroimage.2012.03.081.

Kelly, S. P., Vanegas, M. I., Schroeder, C. E., & Lalor, E. C. (2013). The cruciform model of striate generation of the early VEP, re-illustrated, not revoked: A reply to Ales et al. (2013). *NeuroImage, 82*, 154–159, https://doi.org/10.1016/j.neuroimage.2013.05.112.

Kuai, S. G., & Yu, C. (2006). Constant contour integration in peripheral vision for stimuli with good Gestalt properties. *Journal of Vision, 6*(12):7, 1412–1420, https://doi.org/10.1167/6.12.7.

Lehmann, D., & Skrandies, W. (1979). Multichannel evoked potential fields show different properties of humand upper and lower hemiretina systems. *Experimental Brain Research, 35*(1), 151–159.

Levine, M. W., & Mcanany, J. J. (2005). The relative capabilities of the upper and lower visual hemifields. *Vision Research, 45*, 2820–2830, https://doi.org/10.1016/j.visres.2005.04.001.

Liang, H., Gong, X., Chen, M., Yan, Y., Li, W., & Gilbert, C. D. (2017). Interactions between feedback and lateral connections in the primary visual cortex. *Proceedings of the National Academy of Sciences of the United States of America, 114*(32), 8637–8642, https://doi.org/10.1073/pnas.1706183114.

Liu, T., Heeger, D. J., & Carrasco, M. (2006). Neural correlates of the visual vertical meridian asymmetry. *Journal of Vision, 6*(11):12, 1294–1306, https://doi.org/10.1167/6.11.12.

Marigold, D. S., & Patla, A. E. (2008). Visual information from the lower visual field is important for walking across multi-surface terrain. *Experimental Brain Research, 188*(1), 23–31, https://doi.org/10.1007/s00221-008-1335-7.

McAnany, J. J., & Levine, M. W. (2007). Magnocellular and parvocellular visual pathway contributions to visual field anisotropies. *Vision Research, 47*(17), 2327–2336, https://doi.org/10.1016/j.visres.2007.05.013.

Ofen, N., Moran, A., & Sagi, D. (2007). Effects of trial repetition in texture discrimination. *Vision Research, 47*(8), 1094–1102, https://doi.org/10.1016/j.visres.2007.01.023.

Oostenveld, R., Fries, P., Maris, E., & Schoffelen, J. (2010). FieldTrip: Open source software for advanced analysis of MEG, EEG, and invasive electrophysiological data. *Computational Intelligence and Neuroscience, 2011*, 1–9, https://doi.org/10.1155/2011/156869.

Piëch, V., Li, W., Reeke, G. N., & Gilbert, C. D. (2013). Network model of top-down influences on local gain and contextual interactions in visual cortex. *Proceedings of the National Academy of Sciences of the United States of America, 110*(43), E4108–E4117, https://doi.org/10.1073/pnas.1317019110.

Poghosyan, V., & Ioannides, A. A. (2008). Attention modulates earliest responses in the primary auditory and visual cortices. *Neuron, 58*(5), 802–813, https://doi.org/10.1016/j.neuron.2008.04.013.

Ponce, C. R., Hartmann, T. S., & Livingstone, M. S. (2017). End-stopping predicts curvature tuning along the ventral stream. *Journal of Neuroscience, 37*(3), 648–659, https://doi.org/10.1523/JNEUROSCI.2507-16.2016.

Portin, K., Vanni, S., Virsu, V., & Hari, R. (1999). Stronger occipital cortical activation to lower than upper visual field stimuli. Neuromagnetic recordings. *Experimental Brain Research, 124*, 287–294.

Pourtois, G., Rauss, K. S., Vuilleumier, P., & Schwartz, S. (2008). Effects of perceptual learning on primary visual cortex activity in humans. *Vision Research, 48*(1), 55–62.

Previc, F. H. (1990). Functional specialization in the lower and upper visual fields in humans: Its ecological origins and neurophysiological implications. *Behavioral and Brain Sciences, 13*(03), 519–542, https://doi.org/10.1017/S0140525X00080018.

Quek, G. L., & Finkbeiner, M. (2014). Face-sex categorization is better above fixation than below: Evidence from the reach-to-touch paradigm. *Cognitive, Affective and Behavioral Neuroscience, 14*(4), 1407–1419, https://doi.org/10.3758/s13415-014-0282-y.

R Core Team. R: A language and environment for statistical computing. R Foundation for Statistical Computing. Retrieved from https://www.R-project.org.

Rauss, K., Pourtois, G., Vuilleumier, P., & Schwartz, S. (2009). Attentional load modifies early activity in human primary visual cortex. *Human Brain Mapping, 30*(5), 1723–1733, https://doi.org/10.1002/hbm.20636.

Rauss, K., Pourtois, G., Vuilleumier, P., & Schwartz, S. (2012). Effects of attentional load on early visual processing depend on stimulus timing. *Human Brain Mapping, 33*(1), 63–74, https://doi.org/10.1002/hbm.21193.

Rauss, K., Schwartz, S., & Pourtois, G. (2011). Top-down effects on early visual processing in humans: A predictive coding framework. *Neuroscience and Biobehavioral Reviews, 35*(5), 1237–1253, https://doi.org/10.1016/j.neubiorev.2010.12.011.

Rossi, V., & Pourtois, G. (2012). State-dependent attention modulation of human primary visual cortex: A high density ERP study. *NeuroImage,*

60(4), 2365–2378, https://doi.org/10.1016/j.neuroimage.2012.02.007.

Samonds, J. M., Feese, B. D., Lee, T. S., & Kuhlman, S. J. (2017). Nonuniform surround suppression of visual responses in mouse V1. *Journal of Neurophysiology, 118*(6), 3282–3292, https://doi.org/10.1152/jn.00172.2017.

Schäfer, R., Vasilaki, E., & Senn, W. (2007). Perceptual learning via modification of cortical top-down signals. *PLoS Computational Biology, 3*(8), 1555–1566, https://doi.org/10.1371/journal.pcbi.0030165.

Silva, M. F., Brascamp, J. W., Ferreira, S., Castelo-Branco, M., Dumoulin, S. O., & Harvey, B. M. (2018). Radial asymmetries in population receptive field size and cortical magnification factor in early visual cortex. *NeuroImage, 167*, 41–52, https://doi.org/10.1016/J.NEUROIMAGE.2017.11.021.

Skrandies, W. (1987). The upper and lower visual field of man: Electrophysiological and functional differences. In D. Ottoson (Ed.), *Progress in sensory physiology*, *8*, 1–93. Berlin: Springer.

Slotnick, S. D. (2018). The experimental parameters that affect attentional modulation of the ERP C1 component. *Cognitive Neuroscience, 9*(1–2), 53–62, https://doi.org/10.1080/17588928.2017.1369021.

Timmis, M. A., Bennett, S. J., & Buckley, J. G. (2009). Visuomotor control of step descent: Evidence of specialised role of the lower visual field. *Experimental Brain Research, 195*(2), 219–227, https://doi.org/10.1007/s00221-009-1773-x.

Vater, C., Kredel, R., & Hossner, E. J. (2017). Detecting target changes in multiple object tracking with peripheral vision: More pronounced eccentricity effects for changes in form than in motion. *Journal of Experimental Psychology: Human Perception and Performance, 43*, 903–913.

Vuilleumier, P., Armony, J. L., Driver, J., & Dolan, R. J. (2003). Distinct spatial frequency sensitivities for processing faces and emotional expressions. *Nature Neuroscience, 6*(6), 624–631, https://doi.org/10.1038/nn1057.

Yazdanbakhsh, A., & Livingstone, M. S. (2006). End stopping in V1 is sensitive to contrast. *Nature Neuroscience, 9*(5), 697–702, https://doi.org/10.1038/nn1693.

Zhang, X., An, X., Liu, H., Peng, J., Cai, S., Wang, W., . . . Yang, Y. (2015). The topographical arrangement of cutoff spatial frequencies across lower and upper visual fields in mouse V1. *Scientific Reports, 5*, 1–9, https://doi.org/10.1038/srep07734.

Zhaoping, L. (2009). Perceptual learning of pop-out and the primary visual cortex. *Learning and Perception, 1*(1), 135–146, https://doi.org/10.1556/LP.1.2009.1.10.

Zhou, Y., Yu, G., Yu, X., Wu, S., & Zhang, M. (2017). Asymmetric representations of upper and lower visual fields in egocentric and allocentric references. *Journal of Vision, 17*(1):9, 1–11, https://doi.org/10.1167/17.1.9.

Zito, G. A., Cazzoli, D., Müri, R. M., Mosimann, U. P., & Nef, T. (2016). Behavioral differences in the upper and lower visual hemifields in shape and motion perception. *Frontiers in Behavioral Neuroscience, 10*, 1–8, https://doi.org/10.3389/fnbeh.2016.00128.